ECLOUD'18 SUMMARY*

R. Cimino, LNF-INFN, Frascati, Italy
F. Zimmermann†, CERN, Geneva, Switzerland

Abstract

This article reports some highlights from the joint INFN/ARIES workshop ECLOUD'18. We focus on electron-cloud effects in the LHC and at SuperKEKB, predictions for future machines like FCC-hh, HE-LHC and FCC-ee, models and parameters for the secondary-emission yield, recent trends in electron-cloud simulations, mitigation measures, and novel phenomena. Some workshop statistics and a brief outlook conclude the paper.

INTRODUCTION

ECLOUD'18 [1] was held at La Biodola, Isola d'Elba, from 3 to 7 June 2018. It was jointly organized by INFN [2], CERN [3], the FCC study [4], EuroCirCol [5] and ARIES Work Package 6 APEC [6]. ECLOUD'18 surveyed the state-of-the-art of global electron-cloud research. Topics ranges from electron-cloud build up and effects in particle accelerators and space applications, over beam-induced multipactoring, secondary emission yield models, and surface properties, to mitigation measures and electron-cloud diagnostics. The ECLOUD'18 workshop offered world experts a platform to present and discuss many recent and new electron-cloud observations at the LHC, SuperKEKB, CESR-TA and DAΦNE, and to report and compare electron-cloud predictions for future facilities like FAIR, NICA and the FCC. ECLOUD'18 also showcased and examined electron-cloud mitigation measures, such as clearing electrodes, graphite/carbon coatings, and chemically or laser treated surfaces. In addition, the workshop reviewed the modeling of incoherent electron-cloud effects, self-consistent simulations, and it explored the synergies with other communities like the Valencia Space Consortium and the European Space Agency. Only selected highlights can be presented in the following.

ELECTRON CLOUD IN THE LHC

A big mystery is the unexplained heat-load difference between LHC arc sectors during LHC Run 2 [7], which had not been visible in LHC Run 1 (2010–2012); see Fig. 1. Figure 2 illustrates that the heat load differences appeared between LHC Runs 1 and 2, with four of the LHC sectors showing up to four times higher heat loads after the Long Shutdown 1, which separated Run 1 and Run 2. No correlation had yet been found with any of the shutdown activities. Detailed analyses of local heat loads revealed, in high-load sectors, large differences from cell to cell, and a high heat load in some of the dipole magnets [7, 8]. From simulations, the LHC electron cloud is predicted to be most violent in the quadrupole magnets [9]; for these quadrupoles the presence or absence of photoelectrons does not matter for the heat load [9]. The differences in the heat load could be potentially explained by different surface coverages with CO molecules. Already half a mono-layer of CO can significantly alter the secondary emission yield and its variation with the primary electron energy, as is illustrated in Fig. 3 [10].

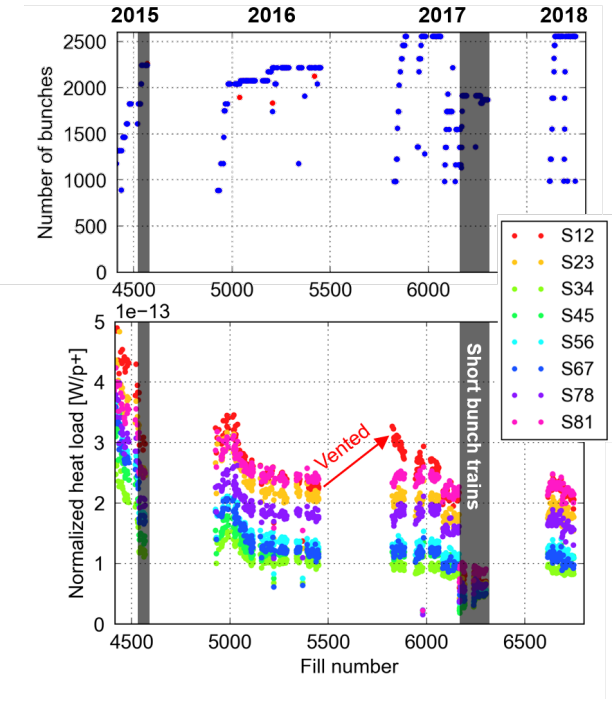

Figure 1: Beam intensity (top) and normalized heat load in the eight LHC arc sectors (bottom) as a function of fill number during almost 4 years of LHC Run 2 operation [7]

The secondary emission yield of LHC beam screens exposed to the proton beam was examined as a function of position [11]. Surprisingly almost no azimuthal dependence is seen, despite the presence of a strong dipole field [11]; the uniformity of the secondary emission yield may also indicate that photoelectrons do not significantly contribute to the surface conditioning. However, these measurements had been taken after keeping the beam screen in air for 1–2 months, which may have resulted in significant deconditioning and/or additional contamination. Measurements during and after white light SR conditioning at a DAΦNE XUV beam line (photon energies 5–1000 eV) show a significant decrease of the secondary electron emission yield (SEY) as a function of photon dose [12], as is documented in Fig. 4. Simulations studies indicate that changes in the orientation and detailed shape of the "sawtooth" surface, on the hori-

* This work was supported in part by the European Commission under the HORIZON 2020 project ARIES no. 730871.
† frank.zimmermann@cern.ch

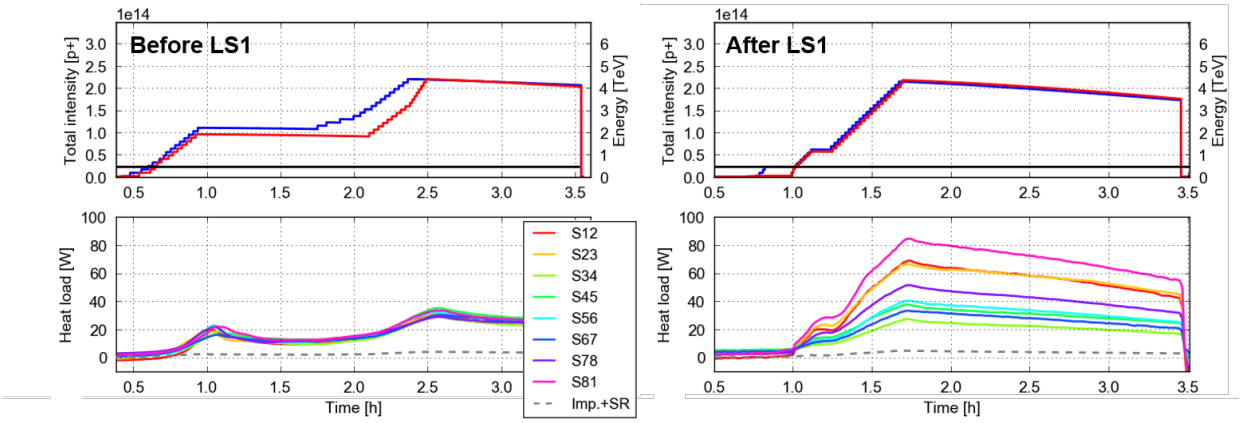

Figure 2: Beam intensity (top) and normalized heat loads (bottom) in the eight LHC arc sectors as a function of time for similar beam parameters before the Long Shutdown 1 (LS1) during Run 1 (left) and after the LS1 in Run 2 (right) [7]

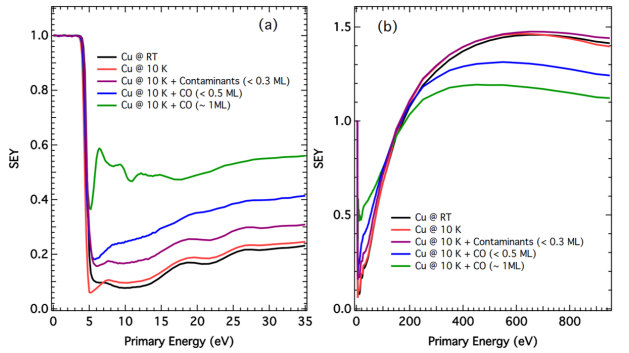

Figure 3: Low-energy (left) and regular secondary emission yield (right) at room temperature (RT) and 10 K, as a function of primary electron energy, for varying surface coverage with contaminants or carbon monoxide of up to one mono-layer (ML) [10].

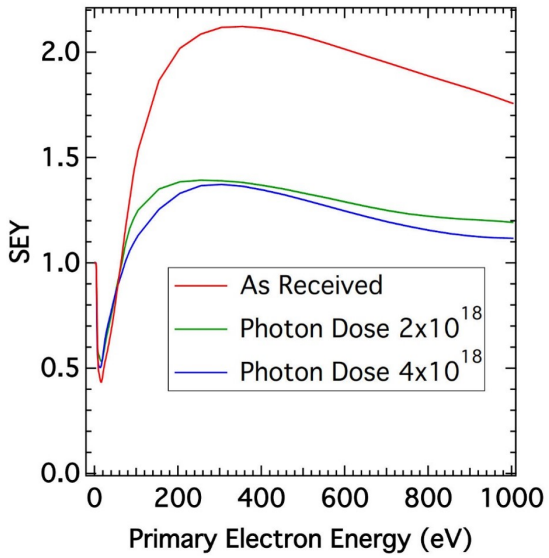

Figure 4: Secondary emission yield for perpendicular incidence of primary electrons as a function of primary energy before, during and after photon conditioning with a total dose of 4×10^{18} mm^{-2} [12].

zontal outward side of the LHC beam screen, can greatly affect the reflectivity and azimuthal distribution of absorbed photons and the resulting electron-cloud heat load [14, 15]. Measurements carried out in the LHC vacuum pilot sector allow discriminating between electron-cloud components caused by synchrotron radiation and due to secondary emission [13]. For a copper surface the secondary emission can contribute two or three orders of magnitude more electrons than primary photoelectrons liberated by synchrotron radiation [13]. These studies also confirmed the electron-cloud reduction by ex-situ NEG coating, and the complete suppression of any electron-cloud build up by amorphous carbon coating [13]

"Post-electron-cloud" simulations include both electrons and ionized molecules, explaining the local beam losses at LHC location "16L2", which is attributed to a local air in-leakage during cooldown. Figure 5 shows the evolution of the simulated ion and electron density during the passage of two successive 48-bunch trains [16]. Synergies of the newly developed multi-specie simulation tool with ITER and other fusion projects [17] and possible applications to muon colliders [18] were highlighted.

SECONDARY EMISSION YIELD STUDIES FOR CSNS

Comprehensive measurements of the angular distribution of the secondary electrons were performed at the CSNS [19]. This complements earlier studies at CERN [20, 21] and at SLAC [22,23]. Figure 6 shows some of the results for various materials. The angular distribution of the secondaries can be parametrised as

$$f(\theta) = \cos\theta(1 + a\sin^2\theta + b\sin^4\theta)\ . \qquad (1)$$

The fitted parameters a and b for different surface materials are summarised in Table 1.

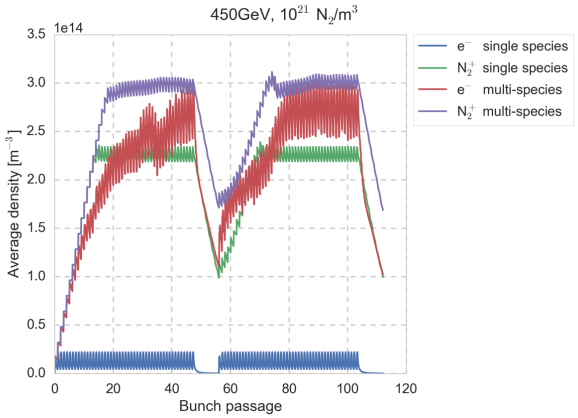

Figure 5: Density of electrons and singly-ionized nitrogen molecules as a function of time in units of bunch passages (the nominal bunch spacing is 25 ns). [16].

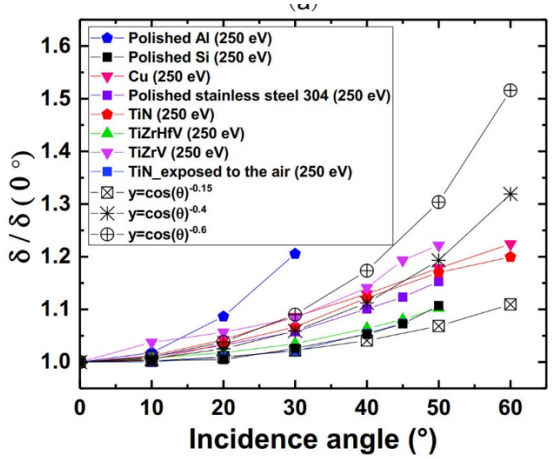

Figure 6: Variation of the secondary emission yield δ with incident angle θ (with respect to the surface normal) [19].

Table 1: Fit parameters characterizing the variation of the secondary emission with the angle of incidence of the primary electron according to Eq. (1), for different surface materials [19].

	a	b
Cu	−2.10	1.63
TiN	−1.24	1.91
TiZrHfV	−1.09	2.03
TiZrV	−0.06	1.99

CLEARING ELECTRODES AT DAΦNE

At DAΦNE, clearing electrodes affected the electron cloud as expected from simulations. Predictions and measurements are compared in Fig. 7. In later times the DAΦNE clearing electrodes were operated with a negative bias voltage [25].

SUPERKEKB

The residual electron cloud in SuperKEKB has been suppressed by many countermeasures, the latest one being permanent-magnet units in any small drift spaces between Phases 1 (2016) and 2 (2018). As far as electron cloud is concerned, SuperKEKB appears well on track towards the design performance. Growth rates measured by the multibunch feedback system [26], vertical beam sizes for close bunch spacing at high positron beam current, up to 600 mA [27], and the pressure rise against the beam current (Fig. 8) [28, 29] all indicate a complete, or nearly complete suppression of electron-cloud build up.

The Phase 2 of SuperKEKB commissioning started in March 2018 [27]. One important ingredient was the squeezing of $\beta^*_{x,y}$ (β^*_x = 200 mm, β^*_y = 4 mm was reached in May 2018). Electron-cloud driven coupled-bunch and single-bunch instabilities were studied in dedicated machine experiments on 29 May. A solenoid-type coupled-bunch instability was observed with a growth time of about 4 ms, that is well suppressed by the bunch-by-bunch feedback system. No single bunch instability (beam size blow-up) was seen up to 0.6 mA/bunch with the design bunch spacing of 4 ns. For comparison, the design bunch current is 1.4 mA. The electron cloud appears to be well controlled [28]. However, the design current is more than a factor two higher than achieved so far and the vertical emittance will be decreased from now 2–3% to the design value of 0.3% during the next year (commissioning phase 3).

Electron-cloud effects in the interaction region (IR) with very high beta is another concern. For the nominal β^* squeeze, the electron density in the IR area should be less than 8×10^{10} m^{-3} to avoid both coherent instability and incoherent emittance growth [27]. Based on a detailed modelling of SuperKEKB synchrotron radiation, including photon scattering, and associated electron-cloud simulations, the electron density in the final superconducting quadrupole QCS was estimated to be as high as, or higher than, 10^{14} m^{-3} [31–33]. Such an electron density could result in a strong instability and emittance growth for the squeezed optics of SuperKEKB.

ELECTRON CLOUD IN FCC-ee

Electron cloud build up in the arcs of the FCC-ee positron ring can be critical, as is illustrated in Fig. 9 [34]. If no care is taken the average heat load due to electron cloud can become comparable to, or exceed, the heat load from synchrotron radiation (about 500 W/m). A maximum secondary emission yield (SEY) below about 1.4–1.5 is required to avoid strong multipacting and to maintain an acceptable load. Such a

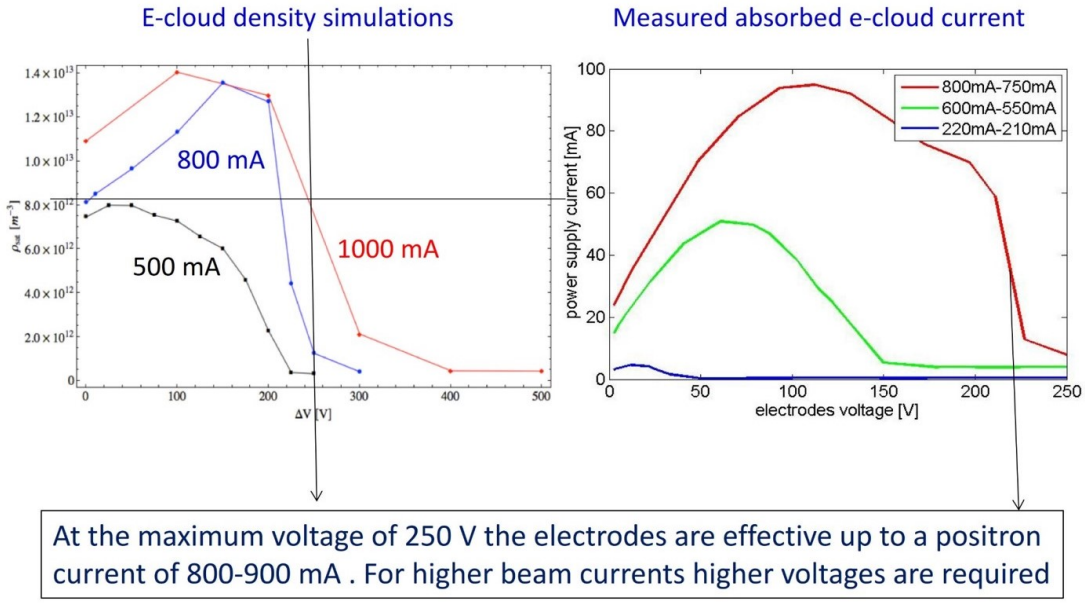

Figure 7: Simulated electron-cloud density (left) and measured electron current (right) as a function of clearing-electrode voltage for different positron beam current in DAΦNE [25].

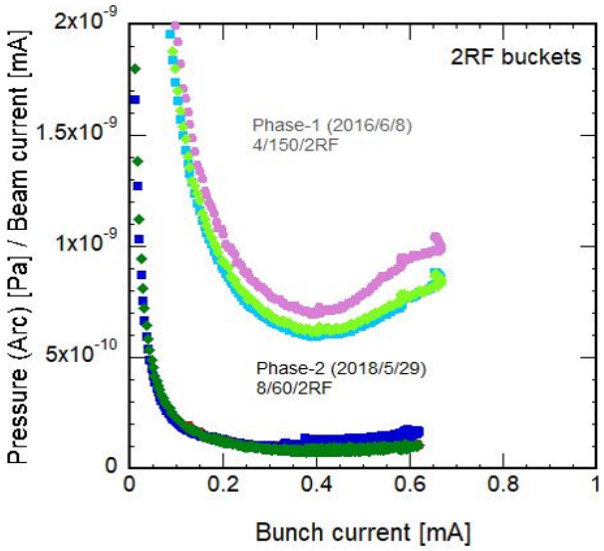

Figure 8: Arc pressure normalised to beam current as a function of beam current in SuperKEKB commissioning phases 1 (2016) and 2 (2018) [28].

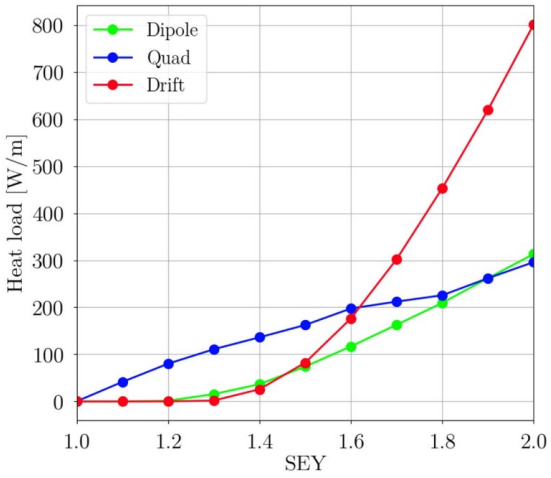

Figure 9: Electron-cloud inducted heat load per unit length for the FCC-ee positron beam in arc dipoles, quadrupoles, and drift spaces [34, 35].

secondary emission yield can be obtained by a NEG coating of the vacuum chamber. On the other hand, the thickness of the NEG coating determines the resistive-wall impedance, and thinner coatings are preferred. The measurements in Fig. 10 shows that novel NEG coatings with a thicknes of only about 100 nm provide the required SEY value even after multiple NEG activations [34, 35].

ELECTRON CLOUD IN HE-LHC AND FCC-hh

The electron cloud in both HE-LHC and FCC-hh is more benign than at the present LHC. Table 2 shows simulated multipacting thresholds in HE-LHC dipoles magnets and drift spaces for the nominal 25 ns bunch spacing, at three different beam energies. Figure 11 shows the simulated heat load in FCC-hh at top energy, as a function of the maximum secondary emission yield, for dipoles, quadrupoles, and drift

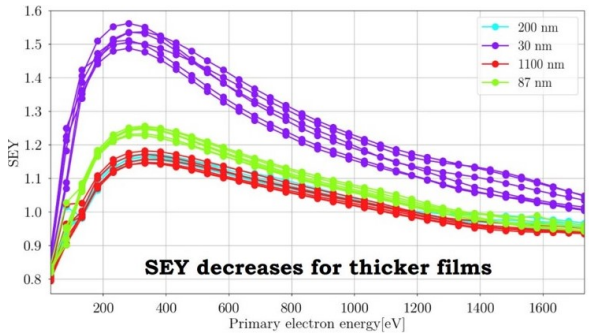

Figure 10: Secondary emission yield, after the fourth NEG activation cycle, as a function of primary electron energy for NEG coating of varying thickness [34, 35].

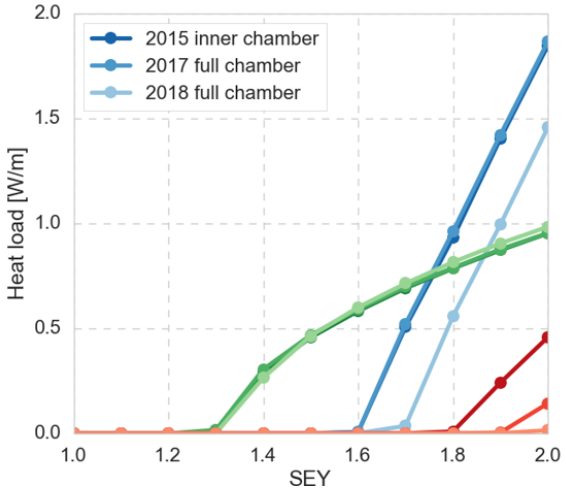

Figure 11: Simulated heat load per unit length in the FCC-hh at top energy (50 TeV per beam) as a function of the maximum secondary emission yield for dipoles (blue), quadrupoles (green), and drift spaces (red) [36].

spaces, considering three different version of the FCC-hh beamscreen.

Table 2: Multipacting thresholds in the HE-LHC arcs from build-up simulations; the threshold is defined as highest SEY without build-up [36].

SEY_{thr}	1.3 TeV inj.	13.5 TeV	13.5 TeV (int. scan)
dipole	1.55	1.45	1.40
drift	1.40	1.45	1.10

A new 2D simulation tool "openEcloud" for electron-cloud studies was developed in Darmstadt [37–39]. The electromagnetic field is calculated with a finite integration technique, using a 2D LU Poisson Solver with arbitrary cut-cell boundaries. A standard particle-in-cell method is employed for the simulation the electron motion, including boundary interaction models. Figure 12 illustrates the de-

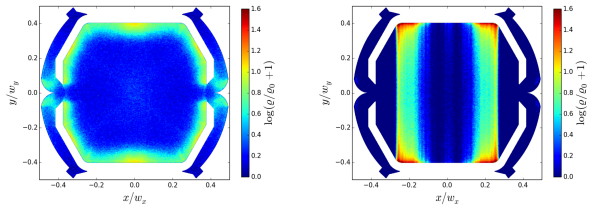

Figure 12: Simulated electron-cloud density for an FCC-hh vacuum chamber with beam screen inside a drift space (left) and a dipole magnet (right) [37].

tailed modelling of the vacuum chamber and shows some example electron distribution for the FCC-hh beam screen in a drift space and inside a dipole magnet,

A transition from Python to Cython programming was advertised [37]. Table 3 summarises simulated multipacting thresholds in LHC and FCC-hh dipole magnets, quadrupole magnets, and drift spaces comparing two different models for the secondary emission. The threshold values in terms of maximum SEY vary greatly with the model. For either model the situation for FCC-hh is more benign than at the LHC, which is consistent with the results of L. Mether [36]. No significant difference is seen between injection and top energy.

Table 3: Multipacting thresholds in the LHC and FCC-hh arcs from build-up simulations comparing the Furman/Pivi [40] and the Cimino/Collins models [21] for the secondary emission yield; the threshold is defined as highest SEY without build-up [37].

	Furman/Pivi		Cimino/Collins	
SEY_{thr}	FCC-hh	LHC	FCC-hh	LHC
dipole	1.25	1.1	1.56	1.32
drift	1.3	1.23	1.6	1.3

A series of thermal desorption spectroscopies has been performed, comparing different levels of surface coverage for common gases [41, 42]. The results in Fig. 13 reveal that the larger the coverage, the lower is the desorption temperature. Binding energies are in the range 100–500 meV and decrease with surface coverage. The question was raised if, given these results, the 60–80 K temperature window is an appropriate choice for the beam screens of HL-LHC, HE-LHC and FCC-hh [42].

LORENTZ BOOSTED FRAME

A frame of reference exists which minimises an aggregate measure of the range of space and time scales for electron-cloud studies [45]. Simulations in a Lorentz boosted frame [44, 45] are illustrated in Fig. 14. This Lorentz boost to an optimised frame allows for much faster and more accurate algorithms and can offer three orders of magnitude

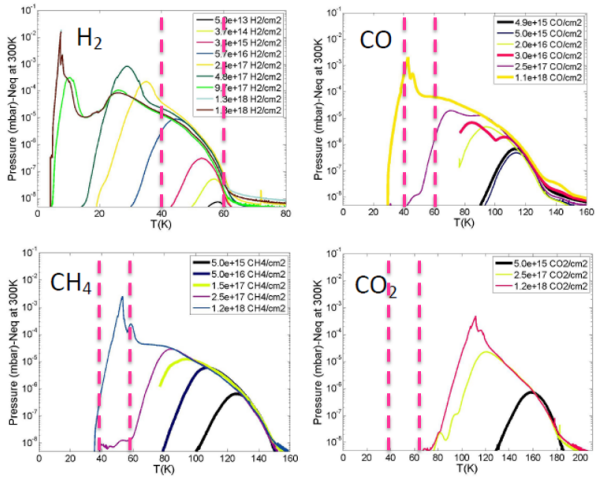

Figure 13: Simulated electron-cloud density for an FCC-hh vacuum chamber with beam screen inside a drift space (left) and a dipole magnet (right) [41, 42].

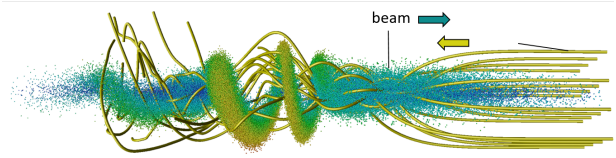

Figure 14: Illustration of an electron-cloud simulation in a Lorentz-boosted frame [44, 45].

gain in computing speed, for a frame with $\gamma^2 = 512$. An arbitrary-order Maxwell solver offers flexibility in accuracy, on centered or staggered grids.

ELECTRON-CLOUD RADIATION

Perhaps inspired by Vay's presentation [44], it was pointed out that in the frame of the beam electrons colliding with protons should lose energy by bremsstrahlung [46]. Photons with energies of order 10–100 keV could be expected in the LHC. With a bremsstrahlung cross section of, for example, $\sigma_{\text{brems}} \approx 10$ mbarn, a proton bunch intensity N_b, and transverse rms beam sizes σ_x and σ_y, the emission probability is of order $\sigma_{\text{brems}} N_b/(\pi\sigma_x\sigma_y) \approx 10^{-9}$ per electron and per proton bunch. An electron cloud line density of order 10^9/m (in the beam rest frame multiplied by γ) with a 25 ns bunch spacing (in the beam rest frame again multiplied by γ) would, back in the laboratory frame, lead to a photon rate of order 50 MHz per meter divided by γ, or 10 kHz per metre. Such "electron-cloud radiation" might be important for the LHC or for the next generation of high-energy hadron colliders.

WORKSHOP STATISTICS

The ECLOUD'18 workshop was attended by 64 experts from around the world. Figure 15 shows the geographical distribution of the ECLOUD'18 participants. In particular, 31% of the participants hailed from the hosting country, Italy, 26% came from nearby Switzerland, and here mostly CERN.

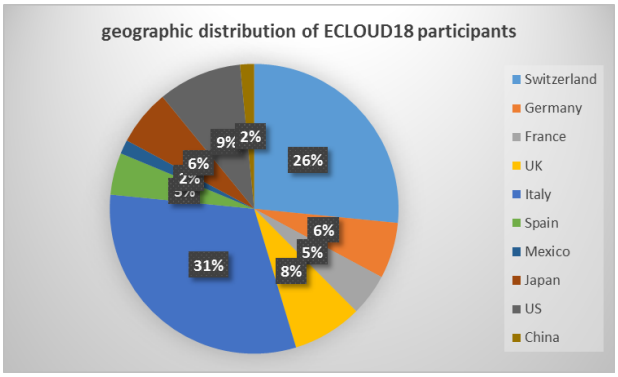

Figure 15: Geographical distribution of ECLOUD'18 participants.

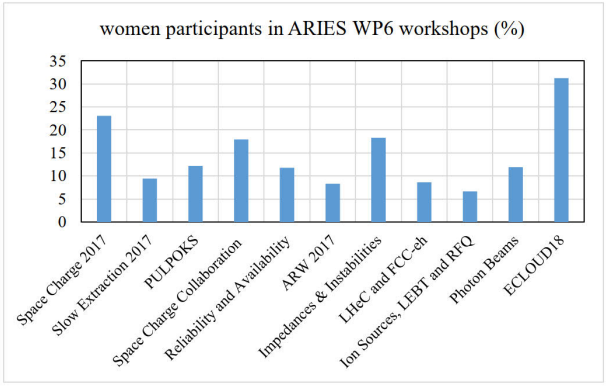

Figure 16: Percentage of women participants for all workshops organized till summer 2018 by ARIES Work Package 6 APEC.

The United States, Japan, UK, Germany and France contributed between 9% and 5% of the participants each. China and Mexico sent 2% each. Figure 16 reveals a rather high fraction of women participants in this workshop devoted to electron-cloud studies, compared with earlier ARIES workshops, which had addressed other topics.

EPILOGUE

ECLOUD'18 presented a superb overview of the present state-of-the-art in electron-cloud modelling and understanding. The remaining challenges, outstanding open questions, and several new approaches were carved out. Electron cloud remains important for the LHC and its upgrade HL-LHC, for SuperKEKB, and for all future high-energy colliders. Another electron-cloud workshop in three years' time (2021) would surely be warranted.

REFERENCES

[1] https://agenda.infn.it/event/13351/

[2] http://www.infn.it

[3] http://www.cern.ch

[4] http://www.cern.ch\fcc

[5] http://eurocircol.eu/

[6] http://aries.web.cern.ch/content/wp6

[7] G. Iadarola, "An Overview on Heat Loads in the LHC", ECLOUD'18, La Biodola, these proceedings.

[8] B. Bradu, "How does a cryogenic system cope with e-cloud induced heat load?", ECLOUD'18, La Biodola, these proceedings.

[9] P. Dijkstal, "Investigating the role of photoemission in the e-cloud formation at the LHC", ECLOUD'18, La Biodola, these proceedings.

[10] L.A. Gonzalez Gomez, "SEY from noble metals", ECLOUD'18, La Biodola, these proceedings and L.A. Gonzalez Gomez, M. Angelucci, R. Larciprete, R. Cimino, "The secondary electron yield of noble metal surfaces", AIP Advances 7, 115203 (2017).

[11] V. Petit, "Characterisation of beam screens extracted from LHC magnets", ECLOUD'18, La Biodola, these proceedings.

[12] M. Angelucci, "Photon Interaction with Technical Surfaces", ECLOUD'18, La Biodola, these proceedings.

[13] E. Buratin, "Preliminary results obtained with the LHC Vacuum Pilot Sector", ECLOUD'18, La Biodola, these proceedings.

[14] G. Guillermo, D. Sagan, and F. Zimmermann, "Examining mitigation schemes for synchrotron radiation in high-energy hadron colliders", Phys. Rev. Accel. Beams 21, 021001 (2018).

[15] G. Guillermo, "Effect of synchrotron radiation and chamber properties on LHC electron-cloud heat load", ECLOUD'18, La Biodola, these proceedings.

[16] G. Iadarola, L. Mether, K. Poland, G. Rumolo, "Post-ecloud regime, challenges for multi-species simulations in beam dynamics", ECLOUD'18, La Biodola, these proceedings.

[17] I. Kaganovich, comment at ECLOUD'18, La Biodola, these proceedings.

[18] R. Cimino, comment at ECLOUD'18, La Biodola, these proceedings.

[19] S. Liu, "SEY studies at CSNS" , ECLOUD'18, La Biodola, these proceedings.

[20] B. Henrist et al., "Secondary Electron Emission Data for the Simulation of Electron Cloud", in Proc. ECLOUD'02, CERN, Geneva, 15–18 April 2002, edited by G. Rumolo and F. Zimmermann, CERN-2002-001 (2002) p. 75.

[21] R. Cimino et al., "Can Low-Energy Electrons Affect High-Energy Physics Accelerators?", Phys. Rev. Lett. 93, 014801 (2004).

[22] M.A. Furman, "The Electron-Cloud Effect in the Arcs of the LHC", LHC-Project-Report-180 (1998).

[23] R.E. Kirby and F.K. King, "Secondary electron emission yields from PEP-II accelerator materials", Nucl. Instrum. Methods Phys. Res. A 469 (2001) 'pp. 1–12.

[24] E. Buratin, "Preliminary results obtained with the LHC Vacuum Pilot Sector" , ECLOUD'18, La Biodola, these proceedings.

[25] C. Milardi, "DAΦNE&ecloud: observations and prospective", ECLOUD'18, La Biodola, this workshop, and D. Alesini D et al. "DAΦNE Operation with Electron-Cloud-Clearing Electrodes" Phys. Rev. Lett. 110 124801

[26] M. Tobiyama, "Coupled-bunch instabilities and related effects due to electron cloud in SuperKEKB LER,", ECLOUD'18, La Biodola, these proceedings.

[27] K. Ohmi, "E-cloud challenges at SuperKEKB and future colliders", ECLOUD'18, La Biodola, these proceedings.

[28] Y. Suetsugu, "ECE and its cures in the SuperKEKB positron ring", ECLOUD'18, La Biodola, these proceedings.

[29] Y. Suetsugu et al., "Mitigating the electron cloud effect in the SuperKEKB positron ring", Phys. Rev. Accel. Beams 22, 023201 (2019).

[30] S.S. Win et al., "Effect of Electron Cloud on the Coupled Bunch Instability in KEKB LER", in Proc. ECLOUD'02, CERN, Geneva, 15–18 April 2002, edited by G. Rumolo and F. Zimmermann, CERN-2002-001 (2002) p. 199.

[31] J. Crittenden, comment at ECLOUD'18, La Biodola, these proceedings.

[32] J.A. Crittenden, D.C. Sagan, T. Ishibashi and Y. Suetsugu, "Synchrotron Radiation Analysis of the SuperKEKB Positron Storage Ring", Proc. IPAC2015 Richmond (2015), p. 2222, http://accelconf.web.cern.ch/AccelConf/IPAC2015/papers/tupty080.pdf

[33] J.A. Crittenden, "Initial Modeling of Electron Cloud Buildup in the Final-Focus Quadrupole Magnets of the SuperKEKB Positron Ring', Proc. IPAC2015 Richmond (2015), p. 2218, http://accelconf.web.cern.ch/AccelConf/IPAC2015/papers/tupty079.pdf

[34] E. Belli, "SEY measurements of coated surfaces with different coating thickness", ECLOUD'18, La Biodola, these proceedings.

[35] E. Belli et al., "Electron cloud buildup and impedance effects on beam dynamics in the Future Circular e+e- Collider and experimental characterization of thin TiZrV vacuum chamber coatings", Phys. Rev. Accel. Beams 21, 111002 (2018).

[36] L. Mether et al., "Electron cloud challenges for future circular machines", ECLOUD'18, La Biodola, these proceedings.

[37] D. Astapovych et al., "E-Cloud Studies for FCC-hh," ECLOUD'18, La Biodola, these proceedings.

[38] https://github.com/openecloud

[39] F. Petrov, O. Boine-Frankenheim, O. Haas, "Interaction of relativistic short proton bunches with space charge limited electron clouds", Phys. Rev. ST Accel. Beams 17, 121001 (2014).

[40] M.A. Furman and M.T.F. Pivi, ÃğProbabilistic model for the simulation of secondary electron emission", Phys. Rev. ST Accel. Beams 5, 124404 (2002).

[41] A.L. Lamure et al., "Adsorption/Desorption from Amorphous Carbon Coating at Cryogenic Temperatures", American Vacuum Society 64th International Symposium and Exhibition (AVS64), Tampa, Florida (2017).

[42] V. Baglin, "Coldex: A tool to study cold surfaces in Accelerators", ECLOUD'18, La Biodola, these proceedings.

[43] L. Spallino, "SEY and other material properties studies at cryogenic temperatures", ECLOUD'18, La Biodola, these proceedings and L. Spallino, M. Angelucci, R. Larciprete and R. Cimino,"On the compatibility of porous surfaces with cryogenic vacuum in future high-energy particle accelerators", Applied Physics Letters 114(15), p. 153103, (2019)

[44] J.-L. Vay, "Progress with 3D modelling of beam dynamics in presence of electron cloud", ECLOUD'18, La Biodola, these proceedings.

[45] J.-L. Vay, "Noninvariance of Space- and Time-Scale Ranges under a Lorentz Transformation and the Implications for the Study of Relativistic Interactionsm", Phys. Rev. Lett. 98, 130405 (2007).

[46] A. Hershcovitch, comment at ECLOUD'18, La Biodola, these proceedings.